



This is a repository copy of *Integrated cardiopulmonary MRI assessment of pulmonary hypertension*.

White Rose Research Online URL for this paper:

<https://eprints.whiterose.ac.uk/202793/>

Version: Published Version

---

**Article:**

Saunders, L.C. [orcid.org/0000-0002-1080-9861](https://orcid.org/0000-0002-1080-9861), Hughes, P.J.C. [orcid.org/0000-0002-7979-5840](https://orcid.org/0000-0002-7979-5840), Alabed, S. [orcid.org/0000-0002-9960-7587](https://orcid.org/0000-0002-9960-7587) et al. (7 more authors) (2022) Integrated cardiopulmonary MRI assessment of pulmonary hypertension. *Journal of Magnetic Resonance Imaging*, 55 (3). pp. 633-652. ISSN 1053-1807

<https://doi.org/10.1002/jmri.27849>

---

**Reuse**

This article is distributed under the terms of the Creative Commons Attribution (CC BY) licence. This licence allows you to distribute, remix, tweak, and build upon the work, even commercially, as long as you credit the authors for the original work. More information and the full terms of the licence here:

<https://creativecommons.org/licenses/>

**Takedown**

If you consider content in White Rose Research Online to be in breach of UK law, please notify us by emailing [eprints@whiterose.ac.uk](mailto:eprints@whiterose.ac.uk) including the URL of the record and the reason for the withdrawal request.



[eprints@whiterose.ac.uk](mailto:eprints@whiterose.ac.uk)  
<https://eprints.whiterose.ac.uk/>

# Integrated Cardiopulmonary MRI Assessment of Pulmonary Hypertension

Laura C. Saunders, PhD,<sup>1</sup>  Paul J. C. Hughes, PhD,<sup>1</sup>  Samer Alabed, MD,<sup>1</sup>  
David J. Capener, BSc,<sup>2</sup> Helen Marshall, PhD,<sup>1</sup> Jens Vogel-Clausen, MD,<sup>3</sup>   
Edwin J. R. van Beek, MD PhD,<sup>4</sup>  David G. Kiely, MD,<sup>1</sup> Andrew J. Swift, MD PhD,<sup>1,2</sup> and  
Jim M. Wild, PhD<sup>1\*</sup>  

If you wish to receive credit for this activity, please refer to the website: [www.wileyhealthlearning.com/JMRI](http://www.wileyhealthlearning.com/JMRI).

## CME Qs for “Integrated cardiopulmonary MRI assessment of pulmonary hypertension”

- Which cardiac MRI markers would indicate poor prognosis in a patient with pulmonary hypertension? (A)
  - Low RV ejection fraction and high RV end systolic volume
  - High LV mass index and high LV stroke volume
  - High RV end diastolic volume and high RV ejection fraction
  - Low RV end-systolic volume and high RV mass index
- Lung perfusion imaging is a promising radiation free diagnostic imaging method to identify which pulmonary hypertension patient group? (D)
  - PH-LHD
  - PAH
  - PH associated with lung disease or hypoxia
  - CTEPH
- Which MRI sequences is best be used to calculate RV and LV volume mass and function? (B)
  - Multi-slice LGE imaging and cine
  - Multi-slice Cine
  - Black blood imaging or 3D phase contrast imaging
  - Cine or black blood imaging
- Roughly how long would a cardiopulmonary MRI examination with dynamic contrast enhanced imaging for a patient with CTEPH take? (B)
  - 20 minutes
  - 1 hour
  - 1 hour 30 minutes
  - 2 hours

View this article online at [wileyonlinelibrary.com](http://wileyonlinelibrary.com). DOI: 10.1002/jmri.27849

Received Feb 26, 2021, Accepted for publication May 24, 2021.

\*Address reprint requests to: J.M.W., Unit of Academic Radiology, floor C, Royal Hallamshire Hospital, University of Sheffield, Glossop Road, Sheffield S10 2JF, UK. E-mail: [j.m.wild@sheffield.ac.uk](mailto:j.m.wild@sheffield.ac.uk),

From the <sup>1</sup>Infection, Immunity and Cardiovascular Disease, University of Sheffield, Sheffield, UK; <sup>2</sup>Imaging, Sheffield Teaching Hospitals, Sheffield, UK; <sup>3</sup>Institute for Diagnostic and Interventional Radiology, Hannover Medical School, Hannover, Germany; and <sup>4</sup>Edinburgh Imaging facility QMRI, University of Edinburgh, Edinburgh, UK

This is an open access article under the terms of the Creative Commons Attribution License, which permits use, distribution and reproduction in any medium, provided the original work is properly cited.

Pulmonary hypertension (PH) is a heterogeneous condition that can affect the lung parenchyma, pulmonary vasculature, and cardiac chambers. Accurate diagnosis often requires multiple complex assessments of the cardiac and pulmonary systems. MRI is able to comprehensively assess cardiac structure and function, as well as lung parenchymal, pulmonary vascular, and functional lung changes. Therefore, MRI has the potential to provide an integrated functional and structural assessment of the cardiopulmonary system in a single exam. Cardiac MRI is used in the assessment of PH in most large PH centers, whereas lung MRI is an emerging technique in patients with PH. This article reviews the current literature on cardiopulmonary MRI in PH, including cine MRI, black-blood imaging, late gadolinium enhancement, T<sub>1</sub> mapping, myocardial strain analysis, contrast-enhanced perfusion imaging and contrast-enhanced MR angiography, and hyperpolarized gas functional lung imaging. This article also highlights recent developments in this field and areas of interest for future research including cardiac MRI-based diagnostic models, machine learning in cardiac MRI, oxygen-enhanced <sup>1</sup>H imaging, contrast-free <sup>1</sup>H perfusion and ventilation imaging, contrast-free angiography and UTE imaging.

**Evidence Level:** 5

**Technical Efficacy:** Stage 3

J. MAGN. RESON. IMAGING 2022;55:633–652.

**P**ULMONARY HYPERTENSION (PH) IS A LIFE-SHORTENING CONDITION and is currently defined by international guidelines as an elevated mean pulmonary arterial pressure (mPAP) of 25 mmHg or higher measured via right heart catheterization,<sup>1</sup> although the recent sixth World Symposium has proposed a new definition of a mPAP of at least 20 mmHg and a pulmonary vascular resistance of at least 3 Wood Units.<sup>2</sup> PH is classified by current guidelines, depending on its underlying causal mechanism, into five sub-categories: 1) pulmonary arterial hypertension (PAH); 2) PH due to chronic left heart disease (PH-LHD); 3) PH due to chronic lung disease and/or hypoxia (PH-Lung); 4) chronic thromboembolic pulmonary hypertension (CTEPH); and 5) unclear or multifactorial causes.<sup>3</sup> The most common types of PH are secondary to chronic heart or lung disease,<sup>3</sup> whereas PAH and CTEPH are rarer forms of PH. PAH is characterized by a primary vasculopathy of the pulmonary arteries, where thickening or stiffening of pulmonary arterioles leads to an increased pulmonary vascular resistance, an increase in the right ventricular (RV) pressure and eventually RV failure. In PH-LHD, chronically raised left atrial pressure results into a secondary elevation of the RV afterload. PH-lung is caused by chronic lung diseases, which restrict the pulmonary vascular bed. In CTEPH nonresolution of clot results in obstruction of the pulmonary vasculature and patients can also develop a vasculopathy similar to PAH in vessels not occluded by chronic clot (Fig. 1).

Currently, there are well-defined treatment options for patients with PAH and CTEPH,<sup>3</sup> whereas for all other forms, treatment is directed at the underlying condition causing PH. Early and accurate diagnosis and categorization of disease is therefore vital for directing patient management and improving outcome, as the underlying form of PH not only defines the approach to treatment but also independently predicts survival.<sup>4</sup>

Right heart catheterization is required to diagnosis PH; however, a multimodal approach is necessary to determine

the etiology of PH. Imaging-based assessments include echocardiography, CT techniques, nuclear medicine methods, and cardiac MRI. Many centers radiological multidisciplinary assessments of PH are still heavily focused around the static structural assessment of the heart and vessels provided by CT and CT pulmonary angiogram (CTPA) with the functional information from MRI of the heart and lungs in PH being underutilized<sup>5,6</sup>; however, a more comprehensive MRI assessment is increasingly being explored.<sup>7,8</sup> MRI has the potential to offer an integrated structural and functional assessment of the entire cardiopulmonary system in one exam and has excellent spatial and temporal resolution without exposure to radiation or invasive heart catheterization. These properties make MRI an ideal tool for the assessment of the etiology, extent of disease and subsequent follow-up of PH patients. In this article, the current state-of-the art of cardiopulmonary MRI in PH is reviewed and possible areas of interest for future research are highlighted. A summary of key outcome measures and associated diagnostic and prognostic threshold values are given in Table 1 and suggested imaging parameters for a cardiopulmonary MRI protocol in PH are given in Table 2.

## CARDIAC MRI: DIAGNOSIS AND PROGNOSIS

Cardiac MRI shows promise as a noninvasive alternative to the diagnostic gold standard of right heart catheterization for diagnosis PH. RV failure (due to high RV pressures and subsequent cardiac remodeling) is considered to be the cause of mortality in patients with PH.<sup>27,28</sup> Therefore, the visualization of the RV structure and function and the interaction of the RV with the other chambers of the heart in particular play a key role in management and assessment of patient prognosis. Cardiac MR-based diagnosis of PH relies on combinations of functional and structural data from cine MRI and velocity information from either black-blood or phase-contrast imaging.

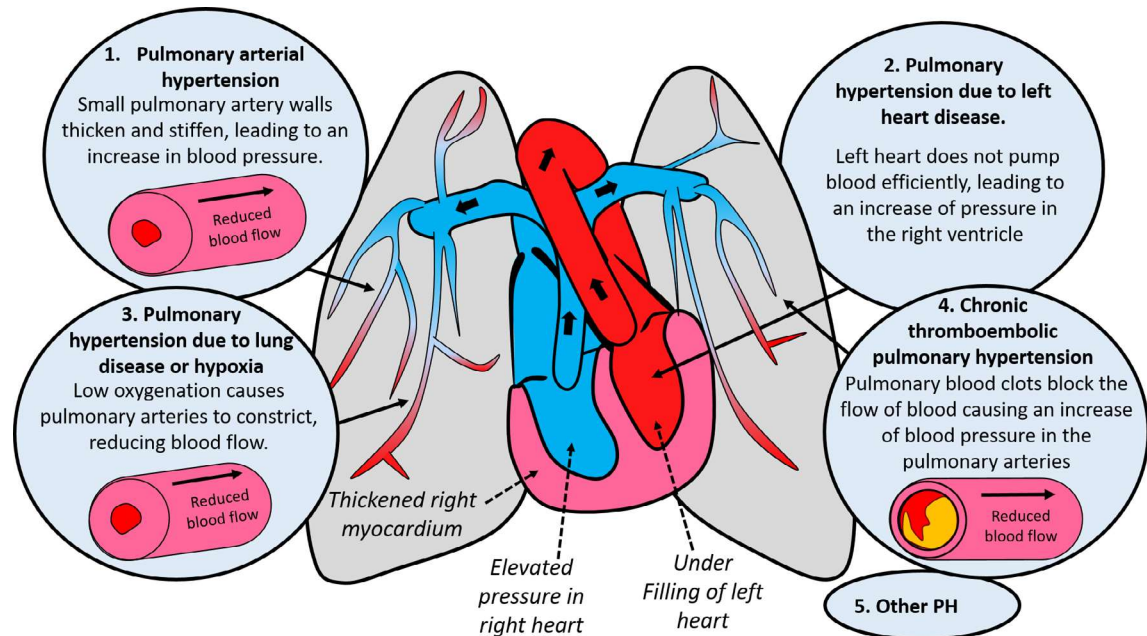


**FIGURE 1:** Schematic diagram showing the key features of PH and the five WHO PH diagnostic groups, which are defined according to underlying cause of PH.

### Cine Cardiac MRI Methods

The elevated pulmonary arterial pressure in patients with PH causes the RV to dilate resulting in a reduction in stroke volume and cardiac output. The RV further adapts to the high pressures through hypertrophy and an increase in the interventricular septal angle (Figs. 2–4). Eventually, the elevated RV pressure and cardiac remodeling cause RV failure.<sup>27,28</sup> Cardiac MR is the gold standard method of visualizing the heart chambers and allows assessment of both RV structure and function.

Cine MRI consists of a stack of cardiac-gated balanced steady-state free precession (bSSFP) images, typically in the short-axis plane covering both ventricles from base to apex. Cine MRI sequences typically use a short echo time, high flip angle and short repetition time to achieve a short acquisition time—resulting in multiple acquisitions per cardiac cycle.<sup>29</sup>

Tracing the endo- and epicardial surfaces on short-axis images during postprocessing allows calculation of RV and left ventricular (LV) volumes contained by the endocardial surfaces, RV end diastolic volume (RVEDV), RV end systolic volume (RVESVI), LV end diastolic volume (LVEDV) and LV end systolic volume (LVESV). RV and LV mass are contained between the endocardial and epicardial surfaces. RV and LV ejection fraction (RVEF and LVEF) and stroke volumes (RVSF and LVSF) can then be calculated. Ventricular mass index (VMI) is calculated as the ratio of the RV and LV mass. Indexed values are calculated for ventricular mass, volumes and function by dividing each value by the patient's body surface area. Intraventricular septal angle can be measured as the angle between the intersection of the interventricular insertion points and interventricular septal

midpoint.<sup>14</sup> In patients with PH, patients typically demonstrate RV dilation and hypertrophy as well as an increased septal angle (Fig. 4).

A study of patients with PAH, using a derivation cohort of 288 and a validation cohort of 288 has shown that RV end systolic volume index has independent prognostic value in PAH.<sup>9</sup> Prognostic threshold values have been identified for cardiac MR measures of cardiac volumes and function. The threshold values of RVESVI > 227% for high-risk patients add prognostic value to the established REVEAL and FRENCH mortality risk calculators.<sup>10</sup> Increased VMI has also been found to correlate with PH severity in studies with 40 systemic sclerosis (SSc) patients (correlation with mPAP  $r = 0.79$ ,  $P < 0.001$ ), 26 patients with suspected PH (correlation with mPAP,  $r = 0.81$ ,  $P < 0.001$ ) and in 64 incident PAH patients VMI was shown to be associated with mortality.<sup>30–32</sup>

A recent publication studying 536 patients with PAH has demonstrated that the way in which heart remodeling takes place can impact survival with a maladaptive response resulting in an increased RV volume relative to VMI mass being associated with poorer worse survival over a mean follow-up time of 5 years (high RVESVI % predicted and low VMI had worse survival than: low RVESVI % predicted and low VMI, HR: 0.390,  $P < 0.001$ ; low RVESVI % predicted and high VMI, HR: 0.260,  $P < 0.001$ ); high RVESVI % predicted and high VMI, HR: 0.524,  $P < 0.001$ ).<sup>11</sup>

Septal angle has been shown to be associated with PH severity and have diagnostic and prognostic value. An increased systolic interventricular septal curvature has been shown to be associated with PH severity in 708 postcapillary

**TABLE 1. Summary of Key Outcome Measures Derived From Cardiopulmonary MRI Protocol for PH**

Wash-in Imaging Method	Key Outcome Measures	Threshold Values Indicative of a PH Diagnosis	Prognostic Threshold Values for Low Risk
Cine cardiac MRI	RV and LV volumes—RVEDVI, RVESVI, LVEDVI, RVESVI		Percentage-predicted RVESVI <180%–227% <sup>9,10</sup>
	RV and LV function—RVEF, LVEF, LVSVI, RSVI		Percentage-predicted RVEF: >54%—low risk <37%—high risk <sup>10</sup>
	Ventricular mass index—VMI		>0.53–0.55 <sup>11</sup>
	Right atrial volume (RAV)		Maximum RAV ≤ 74 mL/m <sup>2</sup> (Ref. 12)
	RA minimal volume index		<30 mL/m <sup>2</sup> (Ref. 13)
	Systolic septal angle		>160° <sup>14</sup>
	Global longitudinal RV strain		>–17% <sup>15</sup>
	Global circumferential RV strain rate		>–0.8 s <sup>–2</sup> (Ref. 15)
Black-blood imaging	Semi-quantitative scoring 0–5	>1 <sup>16</sup>	≥2.5 <sup>16</sup>
Phase-contrast MRI	Average PA velocity		>11.7 cm/sec <sup>17</sup>
	Indexed backward compression wave (children)		<32 mm <sup>5</sup> /sec <sup>18</sup>
	Pulse wave velocity in the main pulmonary artery (children)		<3.1 m/sec <sup>18</sup>
	Indexed forward compression wave (children)		>32 mm <sup>5</sup> /sec <sup>18</sup>
	PWV in patients with COPD and PH		≤7.8 m/sec <sup>19</sup>
	RA reservoir volume index		≥7 mL/m <sup>2</sup> (Ref. 13)
	t <sub>vortex</sub>		≥14.3%–20% depending on method of identification <sup>20,21</sup>
	Area under the backward travelling compression wave	>0.0006 cm <sup>5</sup> for identifying proximal PA clot <sup>22</sup>	
LGE	Qualitative assessment of LGE presence or absence in the right ventricular insertion point		Qualitative assessment of LGE pattern and septal involvement <sup>23</sup>
Perfusion imaging	Pulmonary mean transit time (PTT)		≤6.5 seconds <sup>24</sup>
	FWHM of first pass perfusion		Visual qualitative inspection for CTEPH <sup>25</sup> ≤8 seconds <sup>24</sup>
UTE	%LSV <sub>0.20</sub>	≥17.8% <sup>26</sup> for emphysema	

RV = right ventricular; LV = left ventricular; RVEDVI = RV end diastolic volume index; RVESVI = RV end systolic volume index; LVEDVI = LV end diastolic volume index; LVESVI = LV end systolic volume index; RVEF = RV ejection fraction; LVEF = LV ejection fraction; LVSVI = LV stroke volume index; RSVI = RV stroke volume index; FWHM = full width half maximum.

**TABLE 2. Summary of Suggested Imaging Parameters for PH Assessment**

Sequence	Suggested sequence parameters	Plane, slice position and coverage	Breath hold	Scan time (mm:ss)
Appropriate for all patients				
Axial black blood, cardiac gated spin-echo double inversion recovery	TE: 45 msec TR: 1154 msec FA: 90° Trigger time: 454 msec Percent phase FOV: 90% TI <sub>1</sub> : 50 msec TI <sub>2</sub> : 551 msec Parallel imaging factor: 2	Axial Slices: 4–6 through pulmonary arteries FOV: 400 mm <sup>2</sup> Slice thickness: 8 mm	Insp	01:00
Cardiac cine, balanced steady-state free precession	TE: 1.6 msec TR: 3.7 msec FA: 60° Temporal phases per cardiac cycle: 20 Percent phase FOV: 90% ECG gated	Range of orientations (short axis, four chamber, left ventricle left atrium, right ventricular right atrium, left ventricular outflow tract) Slices: to cover both ventricles from base to apex Slice thickness: 8 mm FOV: 480 mm <sup>2</sup>	Insp	14:00
2D pulmonary artery and aortic Q flow, phase contrast fast gradient echo with velocity encoding	TE: 2.8 msec TR: 5.8 msec FA: 20° FOV: 480 mm <sup>2</sup> Acceleration: Temporal phases per cardiac cycle: 30+ Percent phase FOV: 60% Venc: 150 cm/sec ECG gated	Axial—slice position: one slice orthogonal to the main pulmonary trunk and one orthogonal to the ascending aorta, at the level of the sinotubular junction Slice thickness: 10 mm	Insp	00:30
Suspected left heart disease				
3D SA delayed enhancement, inversion recovery prepped gradient echo	TE: 3.6 msec TR: 7.6 msec FA: 20° Percent phase FOV: 80% TI: 240–280 msec ectypical Contrast agent: 10 min following gadolinium contrast at 0.1 mL/kg ECG gated	Short axis and long axis, repeated after swapping of the phase encode direction. Full ventricular coverage Slice thickness: 8 mm FOV: 480 mm <sup>2</sup>	Exp	00:15

TABLE 2. Continued

Sequence	Suggested sequence parameters	Plane, slice position and coverage	Breath hold	Scan time (mm:ss)
Suspected CTEPH				
3D DCE perfusion, T1-weighted fast gradient echo	TE: 0.7 msec TR: 2.1 msec FA: 30° Parallel imaging factor: 2 Images in acquisition: 3976 Percent phase FOV: 100% Frames: 48 Frame rate: 0.5 seconds Contrast agent: Gadolinium-DTPA at 0.05 mL/kg at a rate of 4 mL/sec	Coronal, full lung coverage Slice thickness: 10 mm FOV: 480 mm <sup>2</sup>	Exp	00:30
3D pulmonary MRA, spoiled gradient echo	TE: 1.3 msec TR: 2.8 msec FA: 30° Parallel imaging factor: 2 Frames per slice: 48 Frame rate: 0.5 seconds Percent phase FOV: 100% Contrast agent: Gadolinium-DTPA at 0.2 mL/kg at a rate of 2 mL/sec	Coronal, to cover pulmonary and thoracic aortic vessels. Slice thickness: 8 mm FOV: 400 mm <sup>2</sup>	Insp	00:10
Or, for contrast-free assessment:				
2D contrast-free perfusion using Fourier Decomposition, balanced steady state free precision.	TE: <0.9 msec (minimal) TR: 3.0 msec FA: 5° Parallel imaging factor: 2 Percent phase FOV: 100% Frames: 250 per slice Frame rate: 0.5 seconds	Multiple coronal and sagittal slices across the lung Slice thickness: 15 mm FOV: 480 mm <sup>2</sup>	Free breathing	05:30
3D contrast-free pulmonary MRA, ECG gated 3D half-Fourier fast spin echo	TE <sub>effective</sub> : 30 msec TR: 3 R-R intervals TI = 190 msec	Coronal, to cover pulmonary and thoracic aortic vessels Slice thickness: 2–4 mm FOV: 256 mm <sup>2</sup>	Intermittent breath hold	03:00
Optional				
	TE: 1.14 msec TR: 3.12 msec	Axial Multislice	Free breathing	06:00–09:00

TABLE 2. Continued

Sequence	Suggested sequence parameters	Plane, slice position and coverage	Breath hold	Scan time (mm:ss)
4D phase-contrast fast gradient echo with velocity encoding	FA: 14° Parallel imaging factor: 2 Temporal resolution: 0.3–0.6 seconds, depends on heart rate. ECG gated			
2D MOLLI—precontrast. Cardiac-gated interleaved inversion recovery with balanced steady-state free precession readout	TE: 0.92 msec TR: 2.8 msec FA: 35°seconds Parallel imaging factor: 2 ECG gated	Short axis Slice thickness: 5 mm FOV: 400 cm <sup>2</sup>	Insp	00:11
2D MOLLI—postcontrast Cardiac-gated interleaved inversion recovery with balanced steady-state free precession readout	TE: 1.0 msec TR: 2.6 msec FA: 35 Parallel imaging factor: 2 ECG gated	Short axis Slice thickness: 5 mm FOV: 400 cm <sup>2</sup>	Insp	00:11
O <sub>2</sub> enhanced T1-weighted inversion recovery	TE: 21 msec TR: 5–6 times R-R TI: 1200 msec Parallel imaging factor: 2 Frames: 80 total, 20 without O <sub>2</sub> enhancement followed by 20 with O <sub>2</sub> enhancement x2. O <sub>2</sub> gas flow delivery 15 liter/min. Contrast: ECG gated	Coronal Multislice Slice thickness: 10 mm FOV: 450 cm <sup>2</sup>	Free breathing	08:00–13:00
Xenon ventilation imaging—MR scanner needs to be configured to work at the frequency of <sup>129</sup> Xe gas	TE: 2.1 msec TR: 6.5 msec FA: 60° Images in acquisition: 28 Percent phase FOV: 80%	Coronal Whole lung coverage Slice thickness: 10 mm FOV: 480 mm <sup>2</sup>	Insp	00:10

PH patients, with elevated septal angle able to identify diastolic pulmonary pressure gradient >7 mmHg with 67% sensitivity and 93% specificity. Septal angle was also predictive of mortality.<sup>14</sup> In 39 patients with PAH systolic pulmonary arterial pressure correlated with systolic septal angle ( $r = 0.77$ ,  $P < 0.001$ ).<sup>33</sup>

While the right atrial area is an established prognostic marker on echocardiogram, it has not been extensively

studied on cardiac MRI. MRI-based right arterial (RA) volume can be measured using multiple methods, including short-axis stacks, four chamber views or cine axial images covering the whole heart. The atrial endocardial maximal and minimal contours can then be drawn on the acquired images, from which volume can be determined. Recent studies suggest that an increase in RA volume is associated with poorer outcomes. In 75 patients with precapillary

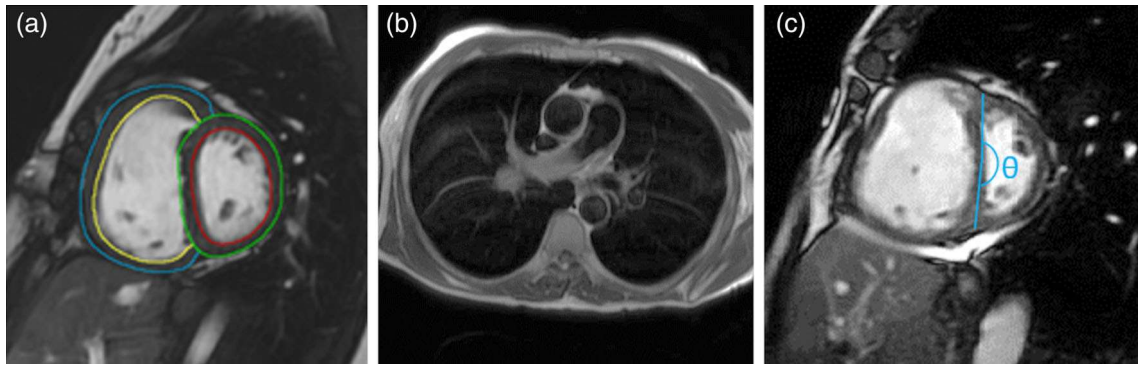


**FIGURE 2:** Combining MR parameters such as cardiac mass, black-blood flow score and interventricular septal angle can increase diagnostic accuracy for PH. (a) Ventricular mass is measured by tracing the endo- and epicardial surfaces on short-axis images. (b) Black-blood imaging can demonstrate dilated pulmonary arteries and areas of reduced blood velocity. (c) Increased interventricular septal angle occurs due to increased RV pressure.

PH and increased right atrial volume (maximum right atrial volume, RAV) decreased survival.<sup>12</sup> In 80 patients with PAH, patients who experienced adverse outcomes (death, prehospitalization or >15% reduction in 6 minute walking distance) had reduced RA emptying fraction.<sup>34</sup> In 68 patients with precapillary PH, clinical worsening (hospitalization due to right heart failure, lung transplantation or PH-related

death) was associated with RA minimum volume index and RA reservoir volume index.<sup>13</sup> Although the studies differed in their method of assessing RA volume, they agreed that RA volume has a role in prognostication of patients with PAH.

Compressed sensing techniques can reduce cine MRI scan time. Compressed sensing techniques undersample k-space during acquisition, and nonlinear iterative

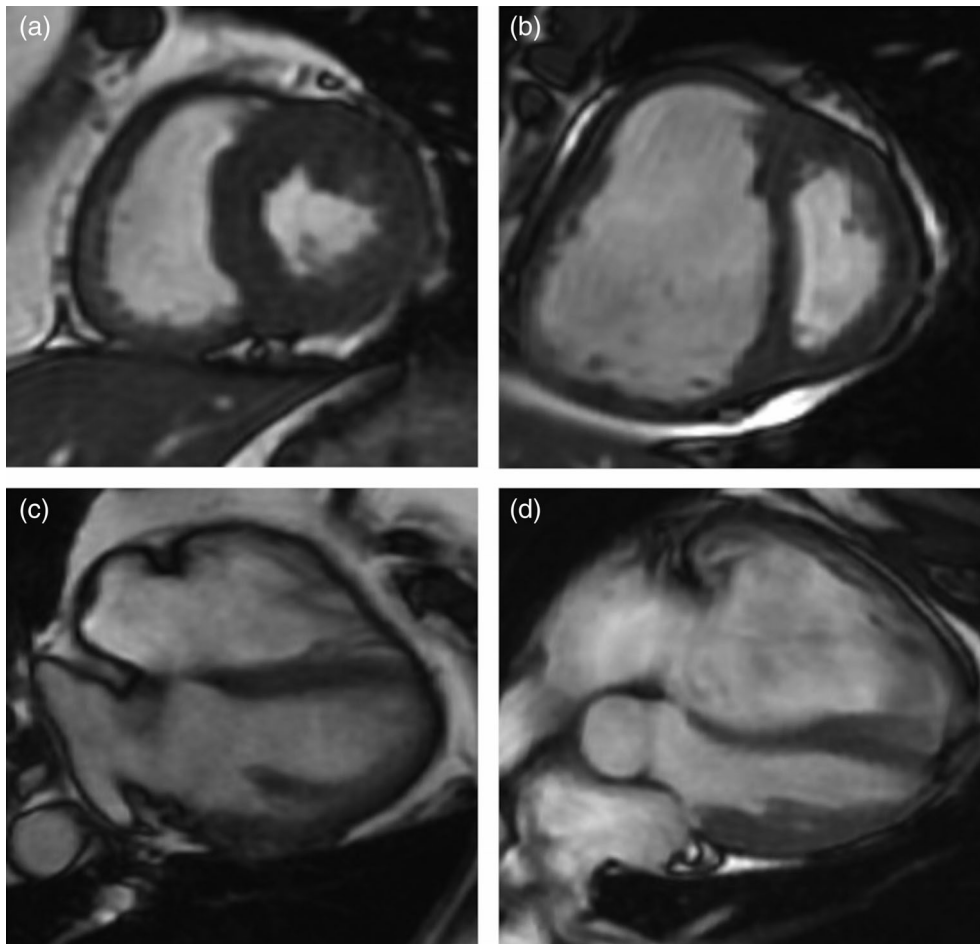


**FIGURE 3:** Short-axis (a,b) and four chamber (c,d) CINE images in a patient without PH (a,c) and a patient with PH (b,d). In patients with PH, elevated RV pressure causes the RV hypertrophy and increased septal angle.

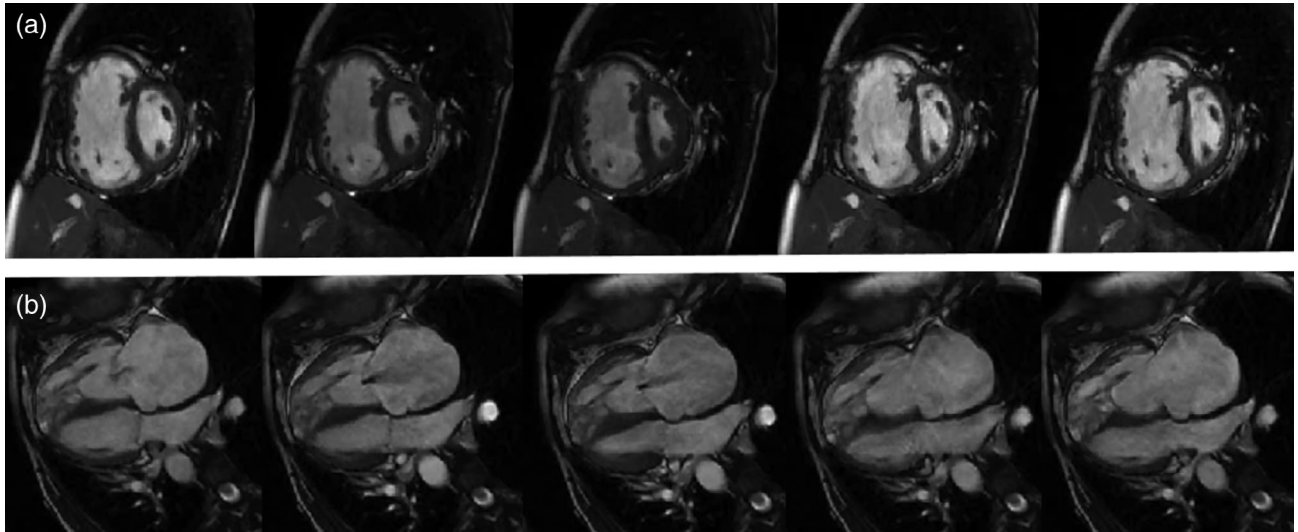


**FIGURE 4:** Short axis (a) and 4 chamber images (b) from the systolic phase of the cardiac cycle in a patient with PH. The interventricular septum is flattened and RV dilatation and hypertrophy can be seen.

reconstruction is used to reduce artefacts, which arise from undersampling.<sup>35</sup> LV and RV mass and function measured from cine MRI images from 81 patients using compressed sensing were found to agree excellently with LV mass and function measured from cine MRI images without compressed sensing with no significant differences in LV volume measurements between the methods, while reducing acquisition time by almost 20 times.<sup>36</sup> Compressed sensing techniques can also be employed to allow free breathing acquisition and have shown to produce comparable results to conventional cine MRI in two studies, one with 26 child or young adult patients and one with 30 child or young adult patients able to perform breath hold and 63 child or young adult patients unable to perform breath holds. However, both studies did show some reduction in image quality.<sup>37,38</sup> The use of image acceleration methods to reduce and eliminate breath holds is particularly

relevant to patients with PH, who may experience dyspnea, as undesired motion during image acquisition can reduce the diagnostic accuracy of the images. Further work evaluating these methods in this patient cohort is therefore warranted.

#### **Blood Flow Methods**

In patients with PH, the increase in pulmonary vascular resistance (PVR) reduces cardiac output, which leads to abnormalities of blood flow in the pulmonary arteries. Slow blood flow in the pulmonary arteries can be visualized using black-blood or phase-contrast MRI.

Black-blood MRI utilizes a gated spin-echo double inversion recovery sequence to null the signal from fast flowing blood, thus highlighting slow flowing blood (Fig. 5). Slices are placed through the pulmonary arteries, which allows the visualization of slow-flowing blood in the pulmonary

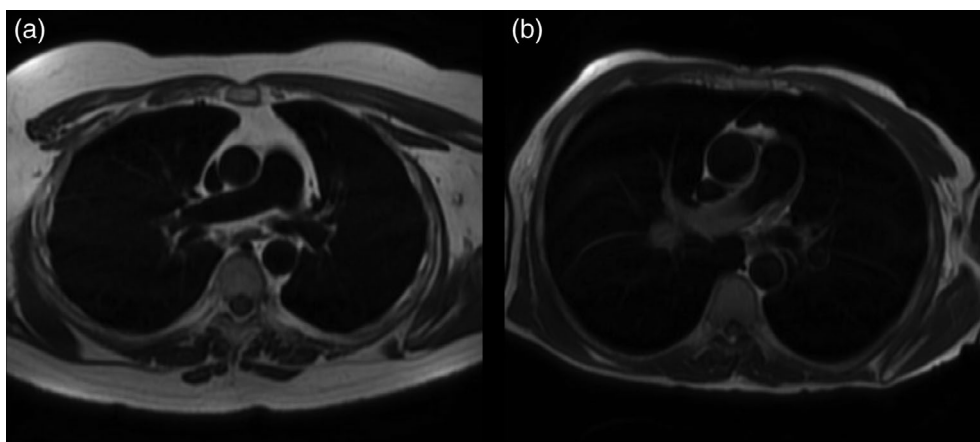


**FIGURE 5:** Black-blood images of the main pulmonary arteries in two patients with suspected pulmonary hypertension. (a) In this patient, no abnormal blood flow can be visualized. (b) In this patient, slow flowing blood can be visualized in the pulmonary artery trunk.

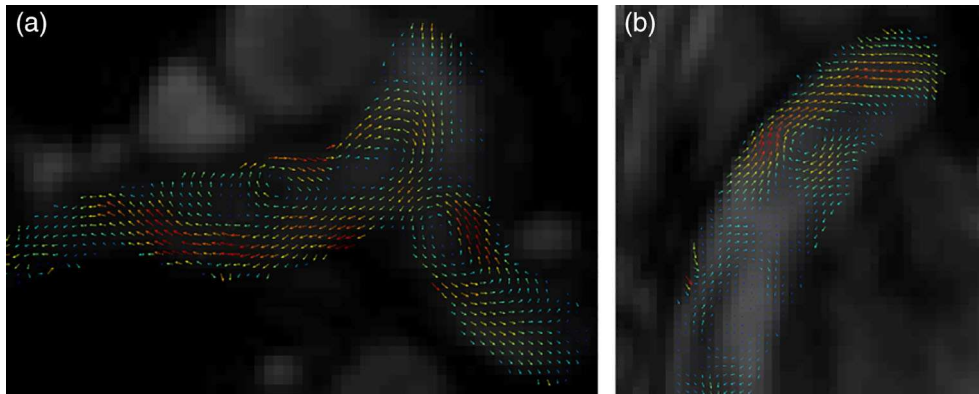


**FIGURE 6:** Visualization of slow blood flow and vortex formation in the pulmonary arteries of two patients with PH (a,b) using a time-resolved phase-contrast imaging sequence.

artery system and dilated central pulmonary arteries. Typical postcontrast inversion times are 50 msec and 550 seconds at 1.5 T. Semi-quantitative scoring can be implemented, which is determined by visual inspection of slow blood patterns by an experienced radiologist.<sup>16</sup> Black-blood imaging can detect dilated central pulmonary arteries as well as areas of reduced blood velocity, and the method has been shown to have a high diagnostic utility in detecting PH in a cohort of 233 patients with suspected PH, with 86% sensitivity and 85% specificity.<sup>16</sup>

While black-blood imaging provides a visual assessment of flow, phase contrast MR allows quantitative assessment of pulmonary arterial blood flow, velocity, and wall motion/strain. Phase-contrast MRI requires gradient echo images to be acquired perpendicular to the main pulmonary artery with velocity encoding in the direction of the pulmonary artery during multiple cardiac phases. For patients with PH, a velocity encoding value of 150 cm/sec is typically used.

During postprocessing, tracing the main pulmonary artery allows the velocity for each voxel to be calculated, with the cyclical pulmonary artery size change allowing the calculation of pulmonary artery dilation and compliance. The area change (AC) of the main pulmonary artery is calculated as difference between the maximum and minimum pulmonary artery areas. The relative area change (RAC) is calculated as a percentage of the mean area of the main pulmonary artery during the cardiac cycle. RAC and AC have both been shown to predict mortality in patients with PH. In a cohort of 134 patients with suspected PH, both AC and RAC predicted mortality.<sup>39</sup> In a cohort of 86 patients with suspected PAH, RAC was significantly lower in survivors ( $P < 0.05$ ) and elevated RAC was associated with increased survival.<sup>17,39</sup>

A reduction in blood velocities and minimum pulmonary artery area has shown good diagnostic accuracy for PAH in a study of 59 patients suspected of having PAH (93% sensitivity, 83% specificity for average velocity, and 93% sensitivity and 88% specificity for minimum pulmonary artery

area).<sup>17</sup> In 145 patients with suspected PH, the duration of vortical blood flow in the main pulmonary artery ( $t_{\text{vortex}}$ , the percentage of cardiac phases with a vortex present) was also able to predict mPAP (linear relationship,  $r = 0.97$ ) and diagnose PH with sensitivity of 97% and specificity of 96%.<sup>20</sup>

Arterial stiffness can also be estimated via pulse wave velocity (PWV), an imaging method utilizing gradient echo phase-contrast images acquired in either a single slice, which captures the descending and ascending aorta, or two slices that capture the aorta a distance  $\Delta d$  apart. The temporal delay  $\Delta t$  between the two waveforms measured and PWV is calculated as  $\Delta d/\Delta t$ .<sup>40,41</sup>

PWV has diagnostic and prognostic value in PH, and measures of arterial stiffness have been found to correlate with PH severity and poor survival. Invasively measured PWV has been shown to be higher in 26 patients with Idiopathic PAH (IPAH) than 10 control subjects ( $P < 0.001$ ).<sup>42</sup> MRI-based wave intensity analysis (WIA) has shown that backward traveling compression waves (BCW) are present in all patients with PH but not healthy controls (20 patients with PH, 10 healthy controls) and that the area under backward traveling compression waves has 100% sensitivity and 91% specificity for the presence of a proximal pulmonary arterial clot in patients with CTEPH.<sup>22</sup> In 40 children with PH and 15 healthy control subjects, BCW magnitude correlates with both invasive and MRI markers of cardiac function including mPAP ( $r = 0.027$ ,  $P = 0.030$ ). In addition, WIA metrics including elevated indexed BCW were associated with increased disease severity.<sup>18</sup> In patients with chronic obstructive pulmonary disease (COPD), PWV has a sensitivity of 94% and specificity of 93% in identifying PH high PWV was associated with poor survival in 30 patients with secondary PH due to COPD.<sup>19</sup>

Phase-contrast MRI can also be applied in three spatial dimensions over time, known as four-dimensional (4D) flow MRI, which allows direct assessment of flow patterns in the cardiac chambers and pulmonary artery and aorta (Fig. 6)

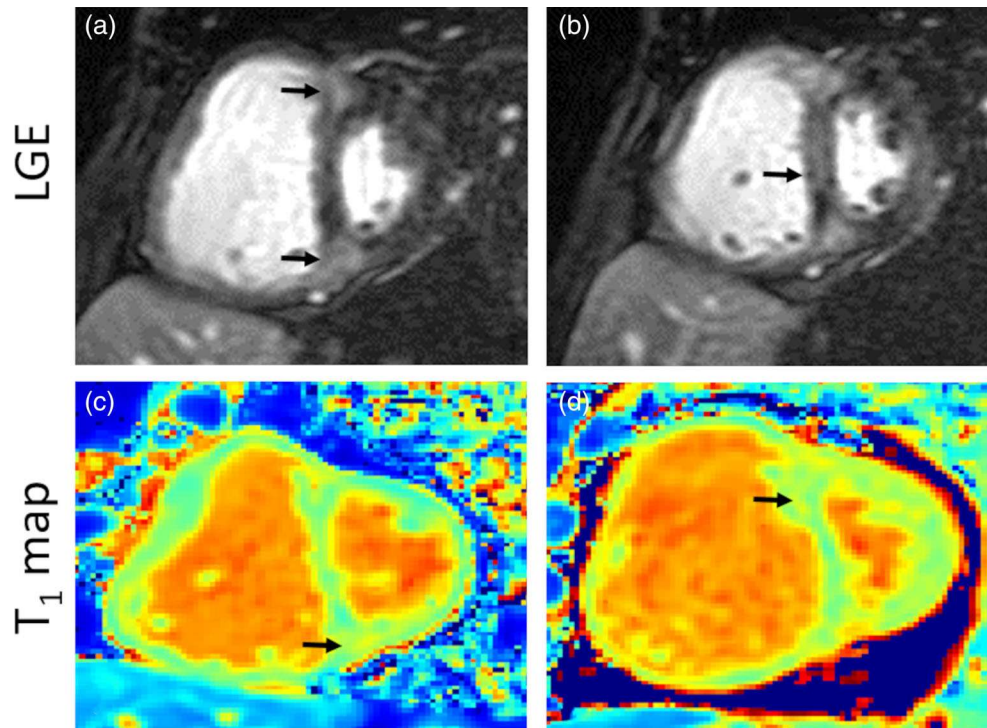


**FIGURE 7:** In patients with PH LGE may be present in the interventricular insertion points alone (a) or in both the interventricular insertion points and extending into the interventricular septum (b). The presence of LGE in the interventricular insertion points is indicative of PH. Native T<sub>1</sub> in the right ventricular insertion points is significantly elevated in patients with PH. Examples of elevated insertion point and septal T<sub>1</sub> in patients with (c) PAH and (d) CTEPH are shown.

alongside cardiac volume and functional measurements. Images are acquired with cardiac and respiratory gating which can result in long scan times (eg, 7:55–14:30 min:sec<sup>43</sup>) and reduced spatial and temporal resolution. Flow velocity is encoded in three directions allowing for a 3D spatial evaluation over time.<sup>43,44</sup>

Abnormal flow patterns in the main pulmonary artery on 4D flow have been associated with the presence and severity of PH. In 23 patients with PH and 27 patients without PH,  $\tau_{\text{vortex}}$  has been demonstrated to have diagnostic utility in PH ( $\tau_{\text{vortex}}$  sensitivity = 96–100%, specificity = 96–100%, depending on method used to determine  $\tau_{\text{vortex}}$ ) and shown to correlate significantly with mPAP ( $r = 0.92$ – $0.95$  depending on method used to determine  $\tau_{\text{vortex}}$ ).<sup>21</sup> Cardiac MRI 4D flow has also been used to assess the pulmonary artery wall shear stress, which can be used as an indicator of vascular remodeling.<sup>45</sup> 4D flow has good agreement with flow calculated using 2D flow MRI; however, 4D flow had a lower area under the ROC curve (AUC) for PA area (2D: AUC = 0.99, 4D: AUC = 0.96) and strain (2D: AUC = 0.93, 4D: AUC = 0.80).<sup>43</sup> Other applications for 4D flow in the assessment of PH include assessment of tricuspid regurgitation or shunts in congenital heart disease.<sup>46</sup>

Flow measurements have been shown to have considerable utility in diagnosis of patients with PH. Combining quantitative variables using linear models has been used to optimize the diagnostic potential of cardiac MRI. A regression

model for MRI-derived mPAP and PVR estimation was produced for nine patients with CTEPH, using a linear combination of metrics (absolute acceleration time, mean velocities, volume of acceleration, and maximum flow acceleration) derived from phase contrast MRI. The goodness of fit of the linear models to the invasively derived mPAP and PVR was 0.892 and 0.792, respectively.<sup>47</sup> A regression model for non-invasively predicting mPAP in patients precapillary PH based on cardiac MRI metrics with a derivation cohort of 270 and a validation cohort of 281 showed that the linear combination of septal angle, VMI and black-blood flow score had superior diagnostic accuracy to the individual parameters alone for identifying patients with mPAP > 20 mmHg and PVR of at least 3 WU. The diagnostic model had a strong agreement with mPAP measured by right heart catheter (intraclass correlation coefficient for estimation of mPAP = 0.78,  $r = 0.80$ ), with AUC was 0.95, 93% sensitivity, and 79% specificity<sup>48</sup> for the diagnosis of PH (defined by an mPAP of at least 25 mmHg). In a recent publication using the same cohort, AUC was 0.93 with 80% sensitivity and 90% specificity for the identification of patients with PH as defined by the sixth World symposium with mPAP greater than 25 mmHg and PVR of at least 3 WU.<sup>49</sup>

### Myocardial Tissue Assessment

The presence of late gadolinium enhancement (LGE) allows the visualization of areas of fibrosis or scarring in the

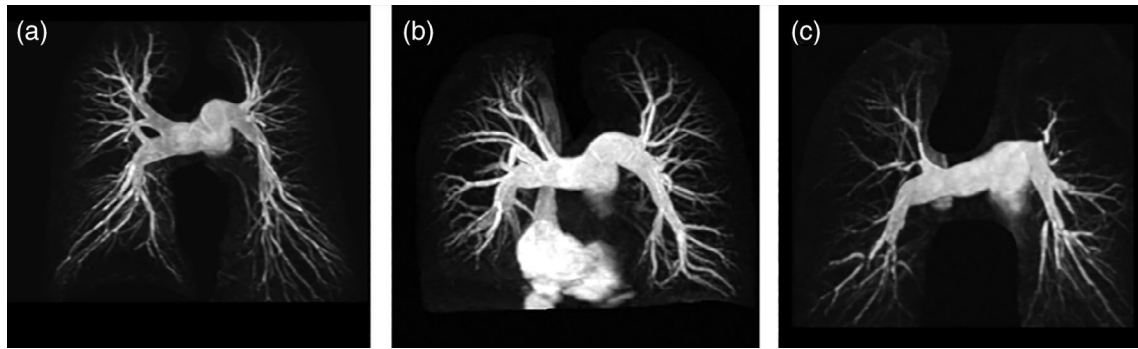


**FIGURE 8:** Examples of MRA in (a) a healthy volunteer, (b) a patient with IPAH, and (c) a patient with CTEPH.

myocardium (Fig. 7). Gadolinium accumulates in the extracellular space of damaged cells within the myocardium. The paramagnetic properties of gadolinium shorten the  $T_1$  of the area in which it accumulates leading to a high signal in a  $T_1$ -weighted image. To capture LGE in patients with PH, gradient echo images are acquired following a  $180^\circ$  inversion, using a short-axis image orientation. Images are typically acquired 10–15 minutes after administration of a gadolinium-based contrast agent. Analysis is based on qualitative assessment of signal increase in the interventricular insertion points and septum by a radiologist.<sup>23</sup>

In PH, LGE is typically seen in the interventricular insertion points and may extend into the interventricular septum. LGE may represent structural tissue changes due to the high RV pressure exerting unusually high strain onto the interventricular septum and has been shown to be associated with RV function, pulmonary hemodynamics and PH severity and prognosis.<sup>50–52</sup> In a cohort of 58 PH patients, LGE presence was shown to be associated with significantly increased RV volume and decreased ejection fraction, and increased mPAP.<sup>52</sup> However, in a cohort of 194 patients with suspected PH, where 192 had PH, although LGE in the intraventricular septum was associated with reduced cardiac function and predicted mortality at 36-month follow-up, the presence of LGE in the RV insertion points is not an independent marker of poor prognosis in PH.<sup>23</sup>

$T_1$  mapping allows quantitative assessment of tissue changes in the myocardium, which can be performed both precontrast and postcontrast.  $T_1$  can be measured by cardiac-gated inversion recovery (IR) or saturation recovery cardiac  $T_1$ -mapping techniques. A commonly used inversion recovery sequence is the Modified Look-Locker Inversion recovery (MOLLI) sequence, which acquires images following three  $180^\circ$  inversions. Postacquisition, images are interleaved into a single recovery curve prior to analysis.<sup>53</sup> Parametric  $T_1$  maps are calculated during postprocessing (Fig. 7), and native (precontrast)  $T_1$  may be a more sensitive indicator of myocardial changes in the presence of PH than LGE.<sup>54</sup> A study with 369 patients with suspected PH (82/369 did not have PH) and 25 age and sex matched healthy volunteers found that  $T_1$

values at the interventricular insertion points are significantly higher in patients with PH compared to healthy volunteers<sup>55</sup>; however, native  $T_1$  did not demonstrate additive value in diagnostic or prognostic evaluation (RV insertion point  $T_1$  did not have additive diagnostic value with  $AUC = 0.654$  and was not associated with mortality,  $P = 0.688$ ).

Myocardial strain analysis on echocardiogram using speckle tracking is capable of predicting mortality in PH.<sup>56</sup> Feature tracking on cardiac MRI uses similar concepts to speckle tracking by tracing the cardiac contours throughout the cardiac cycle on cine imaging. Cardiac MRI can detect strain abnormalities in cardiac chambers that may precede ventricular dysfunction.<sup>57,58</sup> In a cohort of 116 patients with suspected PH, cardiac MRI feature tracking identified that global longitudinal strain (GLS), strain rate (GCSR) and global circumferential strain rate (GCSR) were independently associated with disease severity (GLS and mPAP:  $r = -0.54$ ,  $P < 0.0001$ , GCSR and mPAP:  $r = -0.51$ ,  $P < 0.001$ , GLS and RVEF:  $r = 0.72$ ,  $P < 0.001$ , GCSR and RVEF,  $r = 0.58$ ,  $P < 0.001$ ) and predict patient outcome.<sup>15</sup>

Although tissue assessment methods have been shown to correlate with markers of disease severity in PH, the clinical applications of LGE,  $T_1$  mapping and myocardial strain remain limited in the diagnosis or prognosis of PH as they have not been shown to provide additive diagnostic or prognostic value over established markers of cardiovascular function.

### Image Analysis and Modeling

Machine learning has been rapidly incorporated into registration, reconstruction and segmentation methods in MRI in recent years, which may lead to increased use of MRI metrics in the diagnosis and monitoring of PH. In 72 patients with PH, decision tree analysis using machine learning to combine cardiac MRI parameters has a superior diagnostic performance compared to individual quantitative metrics from 2D phase contrast imaging as well as four chamber and short-axis cine MRI metrics with a sensitivity of 97% and a specificity of 73%.<sup>59</sup> A study using tensor-based machine learning to extract diagnostic features in cardiac MRI without manual segmentation has been implemented in 150 patients with

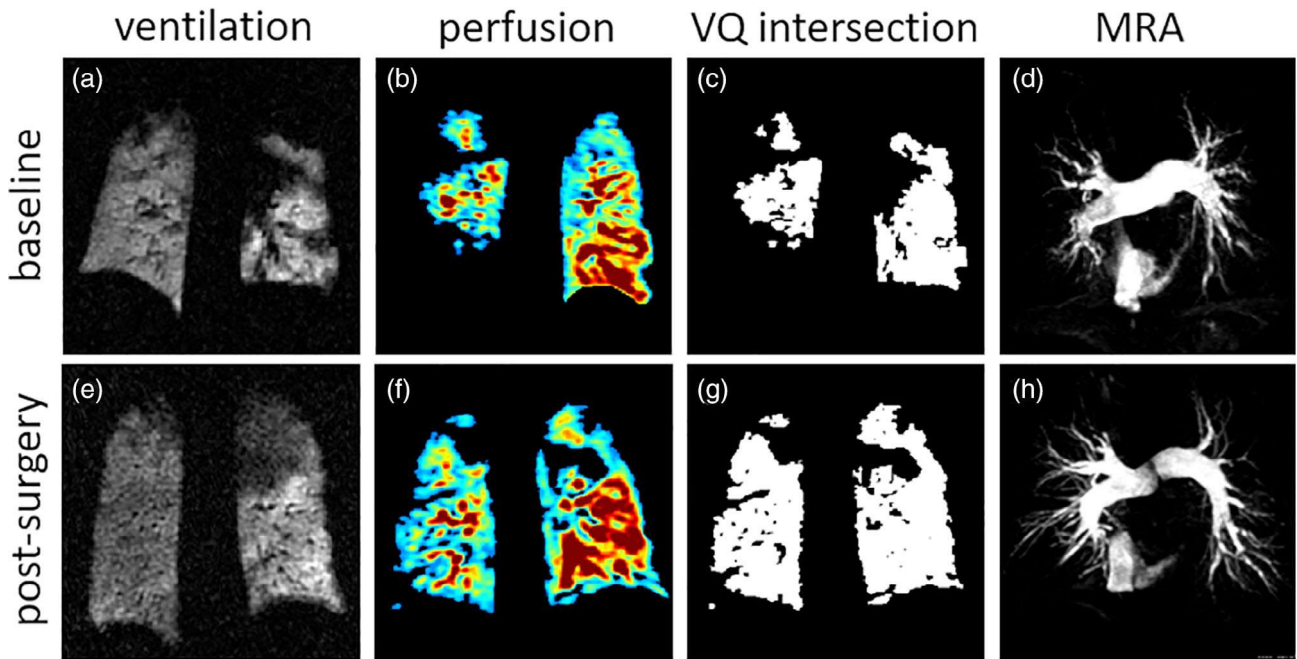


FIGURE 9: MRI ventilation and perfusion (V-Q) matching can be visualized with hyperpolarized  $^3\text{He}$  ventilation (a, e) and gadolinium contrast-enhanced perfusion (b, f). MRI V-Q matching (c, g) and MR angiography (MRA) (d, h) demonstrate treatment response postendarterectomy in patients with CTEPH.

PAH and 70 with no PH,<sup>60</sup> where the machine learning algorithm identified cardiac MRI features associated with PAH and IPAH and successfully distinguished patients from healthy controls (PAH short-axis images, sensitivity 89%, specificity of 81%; IPAH, short-axis image, sensitivity of 93%, specificity of 90%). This machine learning approach provided diagnostic overlay maps to visualize the features identified by the algorithm to indicate a diagnosis of PH. Machine learning is also an emerging technique in prognostic evaluation of PH using MRI. Machine learning assessment of 3D RV motion in 256 patients with newly diagnosed PH was shown to improve outcome prediction when added to a prognostic model including conventional cardiac MRI markers, right heart catheterization data and functional and clinical data (AUC for model including 3D cardiac motion assessment: 0.73, AUC for model without 3D cardiac motion assessment = 0.60,  $P < 0.001$ . Hazard ratio of 3D motion after a median follow-up of 4 years = 2.745,  $P < 0.001$ ).<sup>61</sup>

### PULMONARY VASCULAR MRI: PHENOTYPING AND TREATMENT RESPONSE

A move toward a combined assessment of the cardiac and pulmonary systems in one setting may have higher diagnostic and prognostic performance compared to cardiac MRI alone. Lung MRI is inherently challenging due to the low proton density and short  $T_2^*$  of the healthy lung, resulting in poor visualization of the lung tissue. However, the addition of contrast agents such as gadolinium or hyperpolarized gas improve

the signal-to-noise ratio and allow measurement of functional processes such as lung perfusion and gas transfer, which are physiologically of great interest in the clinical management of PH.

Identifying lung changes is crucial in the assessment of patients with CTEPH, PH due to lung disease or IPAH with mild lung disease. In patients with IPAH, mild lung disease can have a severe impact on prognosis.<sup>62,63</sup>

Dynamic contrast-enhanced (DCE) lung perfusion MRI tracks the passage of a contrast agent (such as gadolinium) through the pulmonary system, allowing the visualization of perfusion defects within the lung. Generally, gadolinium-based contrast agents are used, with dosing varying from 0.05 mL/kg to 0.1 mL/kg and injection rates of 2–4 mL/sec administered through power injectors. Low concentration of the agent ensures sufficient  $T_1$  shortening of the signal in the small blood vessels without excess  $T_2^*$  shortening which would dephase the signal from the already short  $T_2^*$  in the parenchyma (1–2 msec at 1.5 T). In clinical practice, the use of first pass lung DCE can precede a cardiac LGE acquisition resulting in reduced gadolinium dosage for patients.  $T_1$ -weighted gradient echo images are acquired rapidly after the administration of contrast, in order to visualize the movement of the contrast agent through the cardiopulmonary system. Flip angles between  $20^\circ$  and  $40^\circ$  are typically employed to ensure high contrast and signal-to-noise ratios. Typical temporal resolution is  $<1$  seconds, which is achieved through the under sampling of  $k$ -space. Under sampling of  $k$ -space can be carried out using parallel imaging methodologies (GRAPPA and SENSE) with parallel imaging factors of 2–4

most commonly applied. View-sharing reconstruction is also used where high-frequency data from neighboring interleaves are shared to reducing blurring and artifact.<sup>64</sup>

Peak signal enhancement can be calculated for each voxel in a DCE perfusion acquisition, which qualitatively visualizes lung perfusion. Voxel wise blood flow and blood volume can also be calculated by fitting the change in a voxel's signal over time to a model of contrast agent uptake in a voxel over time, with the mean transit time calculated as the pulmonary blood volume divided by the pulmonary blood flow. Lung inflation level affects these lung perfusion metrics, with increased perfusion and reduced transit time seen at expiration when compared with inspiration<sup>65</sup> and large changes seen when comparing breath hold to free breathing perfusion values.<sup>66,67</sup> Valsalva is another issue that can affect pulmonary perfusion metrics.<sup>68</sup>

Decreased or delayed lung perfusion has been shown to have prognostic value in PAH, as well as diagnostic and treatment monitoring value in CTEPH. In 79 patients with PAH, DCE mean pulmonary transit time (PTT, the time difference between the signal peak at the pulmonary artery and left atrium) and full width half maximum of the first pass clearance curve (FWHM) are associated with poorer survival (PTT HR = 1.10,  $P = 0.010$ ; FWHM HR = 1.08,  $P = 0.034$ ). PTT and FWHM are also associated with pulmonary vascular resistance and cardiac index (PTT and PVRI,  $r = 0.720$ ,  $P < 0.0001$ ; PTT and CI,  $r = 0.760$ ,  $P < 0.0001$ ; FWHM and PVRI,  $r = 0.750$ ; FWHM and CI,  $r = 0.780$ ,  $P < 0.0001$ ).<sup>24</sup>

In 74 patients with CTEPH, 3D contrast-enhanced lung perfusion MRI by radiological analysis of the peak enhancement image has been shown to have a high sensitivity of 100% and specificity of 81% in diagnosing CTEPH, which is superior to single-photon emission computed tomography (SPECT) and comparable to computed tomography pulmonary angiogram (CTPA).<sup>25</sup> As MRI does not require ionizing radiation, it has been suggested as the first-line imaging modality in assessing patients with suspected CTEPH.<sup>25</sup> The necessary evidence for the use of lung MRI in the diagnostic pathway of patients with CTEPH is currently being assessed in the ongoing multicenter CHANGE-MRI trial.<sup>69</sup>

A study of 20 patients with CTEPH showed that combined cardiac MRI and DCE MRI exam is suitable for detailed treatment response evaluation before and after pulmonary endarterectomy (PEA) in CTEPH patients, showing an increase lower lobe pulmonary blood flow (PBF) after PEA which correlated with improvement in exercise capacity (6 minute walking distance improvement and change in PBF, spearman  $r = 0.62$ ,  $P = 0.02$ ).<sup>70</sup> DCE MRI of the lung has also been used to assess perfusion treatment response in 29 patients with CTEPH treated with balloon pulmonary angioplasty, where PBF increased significantly in treated lobes

( $P < 0.0001$ ) and nontreated lobes ( $P = 0.015$ ). Change in PBF in the treated lung was shown to correlate with MRI-derived mPAP ( $r = -0.42$ ,  $P = 0.024$ ) and MRI measures of cardiac structure and function (RVEF:  $r = 0.47$ ,  $P = 0.0104$ ; RVSVI:  $r = 0.39$ ,  $P = 0.0372$ ; VMI,  $r = -0.45$ ,  $P = 0.0134$ ), demonstrating the direct relationship between cardiac and pulmonary function.<sup>71</sup>

MR angiography (MRA) visualizes uptake of contrast in the pulmonary vessels. 3D spoiled gradient echo images are acquired in the coronal plane with parallel imaging and view sharing, with a temporal resolution of 0.5–1 seconds per 3D volume. MRA uses higher doses of contrast agent than lung perfusion imaging, around 0.1–0.3 mL/kg. Images are examined qualitatively for pulmonary obstructions or thromboembolic material (Fig. 8). Time-resolved MRA with can be used for bolus timing optimization but may also provide valuable information on cardio-pulmonary blood flow shunting and delayed bronchial circulation.

Patients with IPAH and CTEPH show distinct features on MR angiography allowing patient differentiation and monitoring<sup>29,72</sup> (Figs. 8 and 9). Patients with IPAH may show evidence of vessel pruning (rapid tapering of the vessels) and in patients with CTEPH, MRA can visualize thromboembolic material. In a study of 53 patients with CTEPH, contrast-enhanced MRA has shown excellent sensitivity and specificity (98% and 94%, respectively) in CTEPH diagnosis and is capable of identifying more stenoses, poststenotic dilations and occlusions than CTPA.<sup>73</sup>

### Inhaled Contrast Agent Methods

Techniques utilizing hyperpolarized gas MRI alongside MRI perfusion imaging allow MRI-based ventilation and perfusion imaging (VQ imaging) and assessment of gas transfer in patients with PH (Fig. 9).

Hyperpolarized gas ventilation imaging requires the inhalation of hyperpolarized gas prior to a breath-hold image acquisition. MRI scanners need to be configured to work at the frequency of the <sup>3</sup>He or <sup>129</sup>Xe gas, with specific RF coils also needed. Spin density images of the gas distribution within the lungs visualize areas of ventilated and non-ventilated lung. Analysis can be qualitative, or ventilated areas can be segmented to calculate the percentage of lung volume, which is ventilated. In a study of 15 subjects, good agreement has been shown between scintigraphy ventilation images and <sup>3</sup>He MRI ventilation imaging, with MRI ventilation imaging showing more ventilation defects than scintigraphy. This preliminary work indicates that MRI based ventilation imaging may be a radiation-free alternative for patients with suspected CTEPH.<sup>74</sup> A case study of a woman with CTEPH show that hyperpolarized gas ventilation MRI alongside DCE perfusion MRI has also been used to demonstrate regional ventilation and perfusion treatment response before and after endarterectomy.<sup>75</sup>

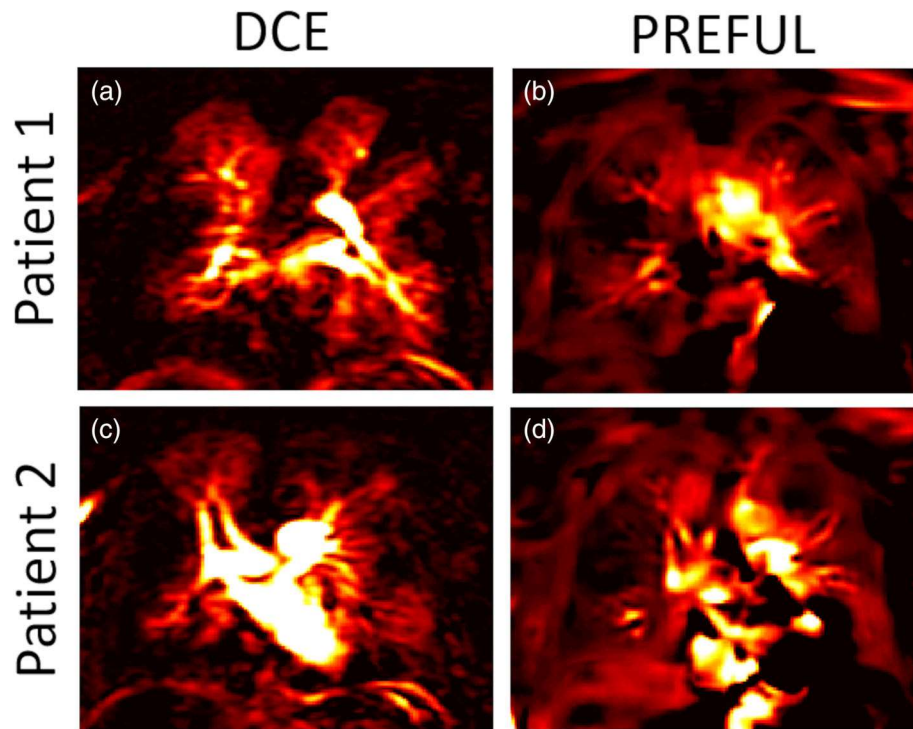


**FIGURE 10:** FD MRI imaging of pulmonary perfusion may offer a contrast-free alternative to DCE. Example peak signal maps from two patients with CTEPH are shown, which were acquired using DCE (a,c) and PREFUL (b,d). Both sets of maps are able to visualize perfusion defects.

$^{129}\text{Xe}$  has advantages over  $^3\text{He}$  including solubility in pulmonary tissues allowing the extraction of gas exchange and alveolar oxygenation using spectroscopy methods. As xenon is soluble in pulmonary tissue, following inhalation the  $^{129}\text{Xe}$  gas dissolves into the pulmonary tissue and blood causing a frequency shift, which can be measured in the MR spectrum.

In two patients with PAH and a patient with CTEPH, hyperpolarized gas MRI has shown well-ventilated lungs, but a decrease in  $^{129}\text{Xe}$  uptake in the red blood cells, indicating perfusion limitation.<sup>76,77</sup> In addition, in a study with 10 patients with PAH, dynamic  $^{129}\text{Xe}$  spectroscopy has shown patients with PAH have increased red blood cell amplitude oscillations, a pattern distinct from patients with left heart failure.<sup>78</sup>

A case study of a patient with CTEPH also indicates that the changes to xenon gas uptake in the red blood cells may also be a useful biomarker in evaluating CTEPH treatment response.<sup>75</sup> Although only a few small studies and case studies have studied the use of hyperpolarized gas MRI in PH, their initial results highlight the potential benefits of MRI-based assessment of V/Q in this patient cohort when combined with DCE MRI of the lung.

Oxygen-enhanced  $^1\text{H}$  MRI uses oxygen as a contrast agent and has been growing in popularity as oxygen is more economical and accessible than hyperpolarized gas, and associated with wider availability and reduced consumables and equipment cost. Acquisition strategies optimize signal from the lung parenchyma and pulmonary vessels with a spin echo

sequence with a short echo time. Patients typically alternate between breathing room air and 100% oxygen during acquisition at 15 liter/min.<sup>79</sup> During postprocessing, an increase in pixel-wise signal due to the paramagnetic properties of the dissolved oxygen within the lung can be calculated as well as the oxygen wash-in and wash-out rates.

In patients 33 with PH, oxygen-enhanced MRI has shown a moderate agreement with V/Q scintigraphy, with a more substantial agreement in ventilation defects than perfusion defects. However only 79% of oxygen-enhanced MRI scans from this study reached a diagnostic level.<sup>80</sup> As oxygen-enhanced MRI appears to represent a combination of ventilation and perfusion information, it may be more challenging to assess the cause of defects using this method. In a study of 12 PH patients, oxygen wash-in time and its interquartile range has been shown to correlate with RV end diastolic volume (wash-in time:  $r = 0.571$ ,  $P = 0.048$ ; wash-in time interquartile range:  $r = 0.857$ ,  $P = 0.0003$ ).<sup>81</sup>

### Noncontrast Lung Perfusion and Angiography

The long-term retention of gadolinium-based contrast agents in the body has raised concerns over its use<sup>82</sup> and driven interest in gadolinium-free alternatives to lung perfusion imaging. Arterial spin labeling (ASL) is an alternative contrast-free proton MRI perfusion method. ASL allows visualization of blood flow without the use of a contrast agent by acquiring two spin echo images, one with a slice-selective  $180^\circ$  inversion and one with a nonselective  $180^\circ$  inversion.

The difference between the two images represents the blood flowing into the slice between the acquisitions and is therefore a measure of blood flow.<sup>83</sup> A study of eight patients with PAH using ASL showed lower blood flow in patients when compared to healthy volunteers.<sup>84</sup>

Fourier decomposition (FD) MRI uses periodic signal intensity changes due to pulsatile blood flow and cyclic respiratory motion to calculate images weighted by lung parenchyma density and perfusion<sup>85</sup> (Fig. 10). 2D free breathing steady-state free precession images are acquired without ECG or respiratory triggering and subsequently undergo nonrigid registration followed by a Fourier transform. Frequency data from the Fourier transform show peaks associated with the periodic cardiac and respiratory motion, which can be isolated and then transformed back into ventilation and perfusion-weighted images. Nonuniform Fourier transformations (NUFD) can be used to compensate for irregular respiratory or cardiac patterns.<sup>86</sup>

There are multiple FD MRI acquisition and processing methodologies available, including SENCEFUL,<sup>87</sup> PREFUL<sup>88</sup> and matrix pencil decomposition.<sup>89</sup> Preliminary work in porcine models has shown that FD MRI can locate ventilation and perfusion defects seen in hyperpolarized gas MRI and DCE MRI<sup>90</sup> and SPECT/CT.<sup>91</sup> PREFUL has been performed in a patient with CTEPH, before and after pulmonary endarterectomy. PREFUL was able to visualize postendarterectomy improvement in hypoperfused lung regions, which visually agreed with DCE perfusion maps.<sup>88</sup> In 30 patients with CTEPH improvement in perfusion weighted PREFUL metrics was been shown to correlate with improvement in 6 minute walking distance ( $r = 0.61$ ,  $P = 0.0031$ ).<sup>92</sup> In addition, in 64 patients with suspected chronic PE, perfusion weighted PREFUL imaging has shown 100% sensitivity and 95% specificity in ruling out or confirming chronic pulmonary embolism (PE) and 94% sensitivity and 94% specificity on a segmental basis.<sup>93</sup> Five patients with suspicion of CTEPH and four with suspected IPAH underwent NUFD and two of those patients demonstrated large perfusion defects, which coincided with defects shown in iodine-enhanced dual-energy CTPA.<sup>86</sup> Initial results from FD MRI are promising; however, larger-scale comparisons of FD MRI to contrast enhanced perfusion and ventilation imaging are warranted to verify its sensitivity.

Contrast-free methods of MRA may allow the visualization the pulmonary vessels without the use of a contrast agent. There are multiple contrast-free MRA methods available including bSSFP techniques, 3D fresh blood imaging using a fast spin echo sequence, radial quiescent-interval slice-selective (QISS) or ASL-based methods.<sup>94</sup>

Contrast-free bSSFP MRA, when used in conjunction with contrast-enhanced MRA, has been shown to improve the overall accuracy of MRA in 53 patients with CTEPH, as it shows clearer differentiation between the vessel wall and

the thromboembolic material adhered to it. However, when considered alone the same study showed that unenhanced bSSFP MRA had poor sensitivity (45%) and a high false positive rate due to the low spatial resolution.<sup>73</sup> For this reason, bSSFP contrast-free MRI is usually used in conjunction with contrast-enhanced MRA.<sup>94</sup>

Radial QISS MRA can be implemented in breath hold and free breathing acquisitions.<sup>95</sup> In 30 patients with acute pulmonary embolism, radial QISS MRA demonstrated increased sensitivity and specificity compared to contrast-free bSSFP MRA (QISS sensitivity = 86.0%, specificity = 93.3%; bSSFP sensitivity = 80.6%, specificity = 84.0%). Further work investigating the use of QISS in chronic pulmonary embolism (CTED) is required to establish whether similar diagnostic accuracy can be achieved in patients with CTEPH and CTED.

3D fresh blood imaging uses an ECG gated 3D half-Fourier fast spin echo sequence. An ECG preparation scan is acquired prior to the 3D fresh blood imaging scan, as different ECG triggering times (i.e. different phases in the cardiac cycle) result in different signal intensity in the blood. An ECG gated 3D spatial labeling method showed unenhanced MRA to be equivalent in diagnostic accuracy, sensitivity, and specificity when compared to contrast-enhanced MRA and contrast-enhanced multidetector CT for assessing pulmonary vasculature in patients with lung cancer.<sup>96</sup> More work is required in this area to explore whether similar unenhanced MRA sequences can also achieve similar diagnostic accuracy in CTEPH patients.

Overall, perfusion imaging in both patients with PAH and CTEPH shows reduced pulmonary blood flow and velocity,<sup>97,98</sup> and perfusion defects.<sup>25,76,86</sup> Blood flow changes in the lungs have been shown to correlate strongly with measures of cardiac structure and function.<sup>71</sup> Therefore, there is a strong argument to evaluate these interconnected systems alongside one another to maximize information on disease etiology and progress. Utilizing all of the information available from MRI exams may provide insight into phenotyping and treatment response, especially if evaluated in an integrated manner using machine learning; however, more work is needed in these areas to robustly establish the effectiveness of these methods.

### Structural Lung Imaging

Patients with PH-lung, or lung disease comorbidity, may benefit from structural imaging of the lung to identify and monitor lung parenchymal changes. Ultra-short echo time (UTE) or zero echo time (ZTE) imaging uses echo times of 0–200  $\mu\text{m}$  to reduce signal loss due to the short  $T_2^*$  of the lung.<sup>99</sup> UTE imaging provides parenchymal contrast and therefore is increasingly being explored as an alternative to CT, particularly when repeat imaging is required.

Although UTE imaging has not been implemented specifically in PH cohorts, chronic obstructive pulmonary disease (COPD) and interstitial lung disease (ILD) are both common causes of PH. Early work in UTE imaging in COPD shows correlations with UTE measures of lung signal and CT measures of lung density. In 15 COPD patients and 5 healthy volunteers, UTE signal intensity was shown to correlate significantly with pulmonary function (forced expiratory volume in 1 second/forced vital capacity [FEV1/FVC],  $r = 0.59$ ,  $P = 0.02$ ) and CT measures of lung density (relative area of the lung with attenuation values  $<950\text{HU}$ ,  $r = -0.71$ ,  $p = 0.005$ ).<sup>100</sup> MRI-based emphysema index was found to correlate with CT-based emphysema index in 10 subjects with COPD and 10 healthy volunteers ( $r = 0.89$ ,  $P < 0.0001$ ).<sup>101</sup> A study in 28 patients with COPD and 10 controls has shown that low-signal-intensity volume had good diagnostic performance in identifying patients with COPD with the percentage of low-signal-intensity volume with an adaptive threshold of 0.20 (%LSV<sub>0.20</sub>) demonstrating 100% sensitivity and 100% specificity.<sup>26</sup> In 18 patients with SSc diagnostic accuracy of MRI-based identification of ILD presence was not significantly different to the diagnostic accuracy of CT (UTE AUC = 0.96, CT AUC = 1.00,  $P = 0.30$ ).<sup>102</sup> In a larger study of 85 patients with varied lung diseases, agreement between pulmonary MR imaging and standard and low dose CT was excellent ( $0.67 \leq \kappa \leq 0.98$ ,  $P < 0.0001$ ).<sup>103</sup> Overall, UTE imaging shows promise in the evaluation of parenchymal changes in patients with COPD and ILD. UTE imaging may be particularly useful in monitoring lung disease and patient follow-up in patients with PH, although further work is warranted in larger cohorts to evaluate this.

## CONCLUSIONS

Integrated cardiopulmonary assessment of patients with PH using MRI offers the potential for diagnosis using combined cardiac MRI metrics of cardiac structure, function and flow. Similarly, prognostic models for patients with PH can be improved by including metrics of structure, function and motion patterns. The use of MRI-based DCE lung perfusion imaging can accurately identify patients with CTEPH and allow treatment monitoring without the use of ionizing radiation. Furthermore, hyperpolarized gas MRI in PAH may display distinct gas transfer patterns that differ from common lung diseases and may provide unique regional pathophysiological insight into mechanism of different PH subgroups and help answer questions such as breathlessness. UTE structural imaging may allow monitoring of lung disease in patients with PH-lung or comorbid lung disease. Utilizing information on both the pulmonary and cardiac systems in one sitting may allow a more thorough evaluation of PH as

well as potentially reducing the need for invasive procedures or exposure to radiation.

## ACKNOWLEDGMENTS

This work was supported by MRC grant MR/M008894/1 and Wellcome Trust grant: 205188/Z/16/Z.

## References

- Galie N, Humbert M, Vachiery JL, et al. ESC/ERS Guidelines for the diagnosis and treatment of pulmonary hypertension The Joint Task Force for the Diagnosis and Treatment of Pulmonary Hypertension of the European Society of Cardiology (ESC) and the European Respiratory Society (ERS) Endorsed by: Association for European Paediatric and Congenital Cardiology (AEPC), International Society for Heart and Lung Transplantation (ISHLT). *Eur Heart J* 2015; 2016;37(1):67.
- Galie N, McLaughlin WV, Rubin LJ, Simonneau G. An overview of the 6th world symposium on pulmonary hypertension. *Eur Respir J* 2019; 53(1):1802148.
- Kiely DG, Elliot CA, Sabroe I, Condliffe R. Pulmonary hypertension: Diagnosis and management. *Bmj-Brit Med J* 2013;346:f2028.
- Hurdman J, Condliffe R, Elliot CA, et al. ASPIRE registry: Assessing the spectrum of pulmonary hypertension identified at a REferral Centre. *Eur Respir J* 2012;39(4):945-955.
- Remy-Jardin M, Ryerson CJ, Schiebler ML, et al. Imaging of pulmonary hypertension in adults: A position paper from the Fleischner society. *Eur Respir J* 2021;57(1):2004455.
- Remy-Jardin M, Ryerson CJ, Schiebler ML, et al. Imaging of pulmonary hypertension in adults: A position paper from the Fleischner society. *Radiology* 2021;57(1):203108.
- Kiely DG, Levin D, Hassoun P, et al. EXPRESS: Statement on imaging and pulmonary hypertension from the pulmonary vascular research institute (PVRI). *Pulm Circ* 2019;9(3):2045894019841990.
- Hatabu H, Ohno Y, Gefter WB, et al. Expanding applications of pulmonary MRI in the clinical evaluation of lung disorders: Fleischner society position paper. *Radiology* 2020;297(2):286-301.
- Swift AJ, Capener D, Johns C, et al. Magnetic resonance imaging in the prognostic evaluation of patients with pulmonary arterial hypertension. *Am J Resp Crit Care* 2017;196(2):228-239.
- Lewis RA, Johns CS, Cogliano M, et al. Identification of cardiac magnetic resonance imaging thresholds for risk stratification in pulmonary arterial hypertension. *Am J Resp Crit Care* 2020;201(4):458-468.
- Goh ZM, Alabed A, Shahin Y, et al. Right ventricular adaptation assessed using cardiac magnetic resonance predicts survival in pulmonary arterial hypertension. *JACC: Cardiovasc Imaging* 2020;14(6):1271-1272.
- Bredfeldt A, Radegran G, Hesselstrand R, Arheden H, Ostenfeld E. Increased right atrial volume measured with cardiac magnetic resonance is associated with worse clinical outcome in patients with pre-capillary pulmonary hypertension. *Esc Heart Fail* 2018;5(5):865-876.
- Sato T, Tsujino I, Ohira H, et al. Right atrial volume and reservoir function are novel independent predictors of clinical worsening in patients with pulmonary hypertension. *J Heart Lung Transplant* 2015;34(3):414-423.
- Johns CS, Wild JM, Rajaram S, et al. Identifying at-risk patients with combined pre- and Postcapillary pulmonary hypertension using Inter-ventricular Septal angle at cardiac MRI. *Radiology* 2018;289(1):61-68.
- de Siqueira MEM, Pozo E, Fernandes VR, et al. Characterization and clinical significance of right ventricular mechanics in pulmonary hypertension evaluated with cardiovascular magnetic resonance feature tracking. *J Cardiovasc Magn R* 2016;18(1):39.

16. Swift AJ, Rajaram S, Marshall H, et al. Black blood MRI has diagnostic and prognostic value in the assessment of patients with pulmonary hypertension. *Eur Radiol* 2012;22(3):695-702.
17. Sanz J, Kuschnir P, Rius T, et al. Pulmonary arterial hypertension: Non-invasive detection with phase-contrast MR imaging. *Radiology* 2007; 243(1):70-79.
18. Schafer M, Wilson N, Ivy DD, et al. Noninvasive wave intensity analysis predicts functional worsening in children with pulmonary arterial hypertension. *Am J Physiol-Heart C* 2018;315(4):H968-H977.
19. Agoston-Coldea L, Lupu S, Mocan T. Pulmonary artery stiffness by cardiac magnetic resonance imaging predicts major adverse cardiovascular events in patients with chronic obstructive pulmonary disease. *Sci Rep* 2018;8(1):14447.
20. Reiter G, Reiter U, Kovacs G, Olschewski H, Fuchsjäger M. Blood flow vortices along the main pulmonary artery measured with MR imaging for diagnosis of pulmonary hypertension. *Radiology* 2015;275(1): 71-79.
21. Reiter U, Reiter G, Kovacs G, et al. Evaluation of elevated mean pulmonary arterial pressure based on magnetic resonance 4D velocity mapping: Comparison of visualization techniques. *PLoS One* 2013;8 (12):e82212.
22. Quail MA, Knight DS, Steeden JA, et al. Noninvasive pulmonary artery wave intensity analysis in pulmonary hypertension. *Am J Physiol-Heart C* 2015;308(12):H1603-H1611.
23. Swift AJ, Rajaram S, Capener D, et al. LGE patterns in pulmonary hypertension do not impact overall mortality. *JACC-Cardiovasc Imag* 2014;7(12):1209-1217.
24. Swift AJ, Telfer A, Rajaram S, et al. Dynamic contrast-enhanced magnetic resonance imaging in patients with pulmonary arterial hypertension. *Pulmonary Circul* 2014;4(1):61-70.
25. Johns CS, Swift AJ, Rajaram S, et al. Lung perfusion: MRI vs. SPECT for screening in suspected chronic thromboembolic pulmonary hypertension. *J Magn Reson Imaging* 2017;46(6):1693-1697.
26. Benlala I, Berger P, Girodet PO, et al. Automated volumetric quantification of emphysema severity by using ultrashort echo time MRI: Validation in participants with chronic obstructive pulmonary disease. *Radiology* 2019;292(1):216-225.
27. Vonk-Noordegraaf A, Haddad F, Chin KM, et al. Right heart adaptation to pulmonary arterial hypertension physiology and pathobiology. *J Am Coll Cardiol* 2013;62(25):D22-D33.
28. Vonk-Noordegraaf A, Galie N. The role of the right ventricle in pulmonary arterial hypertension. *Eur Respir Rev* 2011;20(122):243-253.
29. Swift AJ, Wild JM, Nagle SK, et al. Quantitative magnetic resonance imaging of pulmonary hypertension a practical approach to the current state of the art. *J Thorac Imag* 2014;29(2):68-79.
30. Hagger D, Condliffe R, Woodhouse N, et al. Ventricular mass index correlates with pulmonary artery pressure and predicts survival in suspected systemic sclerosis-associated pulmonary arterial hypertension. *Rheumatology* 2009;48(9):1137-1142.
31. Saba TS, Foster J, Cockburn M, Cowan M, Peacock AJ. Ventricular mass index using magnetic resonance imaging accurately estimates pulmonary artery pressure. *Eur Respir J* 2002;20(6):1519-1524.
32. Simpson CE, Damico RL, Kolb TM, et al. Ventricular mass as a prognostic imaging biomarker in incident pulmonary arterial hypertension. *Eur Respir J* 2019;53(4):1802067.
33. Roelevelt RJ, Marcus JT, Faes TJC, et al. Interventricular septal configuration at MR imaging and pulmonary arterial pressure in pulmonary hypertension. *Radiology* 2005;234(3):710-717.
34. Leng S, Dong Y, Wu Y, et al. Impaired cardiovascular magnetic resonance-derived rapid semiautomated right atrial longitudinal strain is associated with decompensated hemodynamics in pulmonary arterial hypertension. *Circ-Cardiovasc Imag* 2019;12(5):e008582.
35. Lustig M, Donoho D, Pauly JM. Sparse MRI: The application of compressed sensing for rapid MR imaging. *Magn Reson Med* 2007;58(6): 1182-1195.
36. Vermersch M, Longere B, Coisne A, et al. Compressed sensing real-time cine imaging for assessment of ventricular function, volumes and mass in clinical practice. *Eur Radiol* 2020;30(1):609-619.
37. Kocaoglu M, Pednekar AS, Wang H, Alsaied T, Taylor MD, Rattan MS. Breath-hold and free-breathing quantitative assessment of biventricular volume and function using compressed SENSE: A clinical validation in children and young adults. *J Cardiovasc Magn R* 2020;22 (1):54.
38. Pednekar AS, Jadhav S, Noel C, Masand P. Free-breathing cardiorespiratory synchronized cine MRI for assessment of left and right ventricular volume and function in sedated children and adolescents with impaired breath-holding capacity. *Radiology* 2019;1(2):e180027.
39. Swift AJ, Rajaram S, Condliffe R, et al. Pulmonary artery relative area change detects mild elevations in pulmonary vascular resistance and predicts adverse outcome in pulmonary hypertension. *Invest Radiol* 2012;47(10):571-577.
40. Wentland AL, Grist TM, Wieben O. Review of MRI-based measurements of pulse wave velocity: A biomarker of arterial stiffness. *Cardiovasc Diagn Ther* 2014;4(2):193-206.
41. Boese JM, Bock M, Schoenberg SO, Schad LR. Estimation of aortic compliance using magnetic resonance pulse wave velocity measurement. *Phys Med Biol* 2000;45(6):1703-1713.
42. Kopec G, Moertl D, Jankowski P, Tyrka A, Sobien B, Podolec P. Pulmonary artery pulse wave velocity in idiopathic pulmonary arterial hypertension. *Can J Cardiol* 2013;29(6):683-690.
43. Sieren MM, Berlin C, Oechtering TH, et al. Comparison of 4D flow MRI to 2D flow MRI in the pulmonary arteries in healthy volunteers and patients with pulmonary hypertension. *PLoS One* 2019;14(10): e0224121.
44. van der Geest RJ, Garg P. Advanced analysis techniques for intracardiac flow evaluation from 4D flow MRI. *Curr Radiol Rep* 2016;4:38.
45. Barker AJ, Roldan-Alzate A, Entezari P, et al. Four-dimensional flow assessment of pulmonary artery flow and wall shear stress in adult pulmonary arterial hypertension: Results from two institutions. *Magn Reson Med* 2015;73(5):1904-1913.
46. Driessen MMP, Schings MA, Sieswerda GT, et al. Tricuspid flow and regurgitation in congenital heart disease and pulmonary hypertension: Comparison of 4D flow cardiovascular magnetic resonance and echocardiography. *J Cardiovasc Magn Reson* 2018;20(1):5.
47. Kreitner KF, Wirth GM, Krummenauer F, et al. Noninvasive assessment of pulmonary hemodynamics in patients with chronic thromboembolic pulmonary hypertension by high temporal resolution phase-contrast MRI correlation with simultaneous invasive pressure recordings. *Circ-Cardiovasc Imag* 2013;6(5):722-729.
48. Johns CS, Kiely DG, Rajaram S, et al. Diagnosis of pulmonary hypertension with cardiac MRI: Derivation and validation of regression models. *Radiology* 2019;290(1):61-68.
49. Whitfield AJ, Solanki R, Johns CS, Kiely D, Wild J, Swift AJ. MRI prediction of precapillary pulmonary hypertension according to the sixth world symposium on pulmonary hypertension. *Radiology* 2020;294(2): 482-482.
50. Blyth KG, Groenning BA, Martin TN, et al. Contrast enhanced-cardiovascular magnetic resonance imaging in patients with pulmonary hypertension. *Eur Heart J* 2005;26(19):1993-1999.
51. Shehata ML, Lossnitzer D, Skrok J, et al. Myocardial delayed enhancement in pulmonary hypertension: Pulmonary hemodynamics, right ventricular function, and remodeling. *Am J Roentgenol* 2011;196(1): 87-94.
52. Freed BH, Gomberg-Maitland M, Chandra S, et al. Late gadolinium enhancement cardiovascular magnetic resonance predicts clinical worsening in patients with pulmonary hypertension. *J Cardiovasc Magn Reson* 2012;14:11.
53. Messroghli DR, Radjenovic A, Kozerke S, Higgins DM, Sivanathan MU, Ridgway JP. Modified look-locker inversion recovery (MOLLI) for high-resolution T-1 mapping of the heart. *Magn Reson Med* 2004;52(1):141-146.

54. Garcia-Alvarez A, Garcia-Lunar I, Pereda D, et al. Association of myocardial T1-mapping CMR with hemodynamics and RV performance in pulmonary hypertension. *JACC-Cardiovasc Imag* 2015;8(1):76-82.
55. Saunders LC, Johns CS, Stewart NJ, et al. Diagnostic and prognostic significance of cardiovascular magnetic resonance native myocardial T1 mapping in patients with pulmonary hypertension. *J Cardiovasc Magn R* 2018;20.
56. Shukla M, Park JH, Thomas JD, et al. Prognostic value of right ventricular strain using speckle-tracking echocardiography in pulmonary hypertension: A systematic review and meta-analysis. *Can J Cardiol* 2018;34(8):1069-1078.
57. Lin ACW, Seale H, Hamilton-Craig C, Morris NR, Strugnell W. Quantification of biventricular strain and assessment of ventriculo-ventricular interaction in pulmonary arterial hypertension using exercise cardiac magnetic resonance imaging and myocardial feature tracking. *J Magn Reson Imaging* 2019;49(5):1427-1436.
58. Shehata ML, Harouni AA, Skrok J, et al. Regional and global biventricular function in pulmonary arterial hypertension: A cardiac MR imaging study. *Radiology* 2013;266(1):114-122.
59. Lungu A, Swift AJ, Capener D, Kiely D, Hose R, Wild JM. Diagnosis of pulmonary hypertension from magnetic resonance imaging-based computational models and decision tree analysis. *Pulmonary Circul* 2016;6(2):181-190.
60. Swift AJ, Lu H, Uthoff J, et al. A machine learning cardiac magnetic resonance approach to extract disease features and automate pulmonary arterial hypertension diagnosis. *Eur Heart J Cardiovasc Imaging* 2020.
61. Dawes TJW, de Marvao A, Shi W, et al. Machine learning of three-dimensional right ventricular motion enables outcome prediction in pulmonary hypertension: A cardiac MR imaging study. *Radiology* 2017;283(2):381-390.
62. Peacock AJ, Ling Y, Johnson MK, et al. Idiopathic pulmonary arterial hypertension and co-existing lung disease: Is this a new phenotype? *Pulm Circ* 2020;10(1):2045894020914851.
63. Lewis RA, Thompson AAR, Billings CG, et al. Mild parenchymal lung disease and/or low diffusion capacity impacts survival and treatment response in patients diagnosed with idiopathic pulmonary arterial hypertension. *Eur Respir J* 2020;55(6).
64. Du J. Contrast-enhanced MR: Angiography using time resolved interleaved projection sampling with three-dimensional Cartesian phase and slice encoding (TRIPPS). *Magn Reson Med* 2009;61(4):918-924.
65. Fink C, Ley S, Risse F, et al. Effect of inspiratory and expiratory breath-hold on pulmonary perfusion: Assessment by pulmonary perfusion magnetic resonance imaging. *Invest Radiol* 2005;40(2):72-79.
66. Maxien D, Ingrisch M, Meinel F, Reiser M, Dietrich O, Nikolaou K. Quantification of pulmonary perfusion with free-breathing dynamic contrast-enhanced MRI—a pilot study in healthy volunteers. *RoFo* 2013; 185(12):1175-1181.
67. Ingrisch M, Maxien D, Schwab F, Reiser MF, Nikolaou K, Dietrich O. Assessment of pulmonary perfusion with breath-hold and free-breathing dynamic contrast-enhanced magnetic resonance imaging: Quantification and reproducibility. *Invest Radiol* 2014;49(6):382-389.
68. Eichenberger A, Schwitter J, McKinnon G, Debatin J, Von Schulthess G. Phase-contrast echo-planar MR imaging: Real-time quantification of flow and velocity patterns in the thoracic vessels induced by valsalva's maneuver. *J Magn Reson Imaging* 1995;5(6): 648-655.
69. Lasch F, Karch A, Koch A, et al. Comparison of MRI and VQ-SPECT as a screening test for patients with suspected CTEPH: CHANGE-MRI study design and rationale. *Front Cardiovasc Med* 2020;7:51.
70. Schoenfeld C, Cebotari S, Hinrichs J, et al. MR imaging-derived regional pulmonary parenchymal perfusion and cardiac function for monitoring patients with chronic thromboembolic pulmonary hypertension before and after pulmonary endarterectomy. *Radiology* 2016; 279(3):925-934.
71. Schoenfeld C, Hinrichs JB, Olsson KM, et al. Cardio-pulmonary MRI for detection of treatment response after a single BPA treatment session in CTEPH patients. *Eur Radiol* 2019;29(4):1693-1702.
72. Junqueira FP, Lima CM, Coutinho AC Jr, et al. Pulmonary arterial hypertension: An imaging review comparing MR pulmonary angiography and perfusion with multidetector CT angiography. *Br J Radiol* 2012;85(1019):1446-1456.
73. Rajaram S, Swift AJ, Capener D, et al. Diagnostic accuracy of contrast-enhanced MR angiography and unenhanced proton MR imaging compared with CT pulmonary angiography in chronic thromboembolic pulmonary hypertension. *Eur Radiol* 2012;22(2):310-317.
74. Altes TA, Rehm PK, Brookeman JR, Truwit JD, De Lange EE. Ventilation imaging of the lung: Comparison of hyperpolarized helium-3 MR and xenon-133 scintigraphy. *Radiology* 2001;221:563-563.
75. Marshall H, Kiely DG, Parra-Robles J, et al. Magnetic resonance imaging of ventilation and perfusion changes in response to pulmonary endarterectomy in chronic thromboembolic pulmonary hypertension. *Am J Respir Crit Care Med* 2014;190(5):e18-e19.
76. Wang ZY, He M, Bier E, et al. Hyperpolarized Xe-129 gas transfer MRI: The transition from 1.5T to 3T. *Magn Reson Med* 2018;80(6): 2374-2383.
77. Dahhan T, Kaushik SS, He M, et al. Abnormalities in hyperpolarized Xe-129 magnetic resonance imaging and spectroscopy in two patients with pulmonary vascular disease. *Pulmonary Circul* 2016;6(1):126-131.
78. Wang ZY, Bier EA, Swaminathan A, et al. Diverse cardiopulmonary diseases are associated with distinct xenon magnetic resonance imaging signatures. *Eur Respir J* 2019;54(6).
79. Mai VM, Liu B, Li W, et al. Influence of oxygen flow rate on signal and T-1 changes in oxygen-enhanced ventilation imaging. *J Magn Reson Imaging* 2002;16(1):37-41.
80. Maxien D, Dietrich O, Thieme SF, et al. Value of oxygen-enhanced MRI of the lungs in patients with pulmonary hypertension: A qualitative and quantitative approach. *J Magn Reson Imaging* 2012;35(1): 86-94.
81. Sathianandan S, Rawal B, Price L, et al. Dynamic oxygen-enhanced magnetic resonance imaging-based quantification of pulmonary hypertension. *Eur Respir J* 2020;56.
82. Kanal E. Gadolinium based contrast agents (GBCA): Safety overview after 3 decades of clinical experience. *Magn Reson Imaging* 2016;34 (10):1341-1345.
83. Hopkins SR, Prisk GK. Lung perfusion measured using magnetic resonance imaging: New tools for physiological insights into the pulmonary circulation. *J Magn Reson Imaging* 2010;32(6):1287-1301.
84. Prisk G, Elliott AR, Pazar B, Kim NH, Hopkins SR. The pulmonary blood flow distribution measured with MRI shows large regions with undetectable flow in PAH patients. *Am J Respir Crit Care Med* 2018;197.
85. Bauman G, Puderbach M, Deimling M, et al. Non-contrast-enhanced perfusion and ventilation assessment of the human lung by means of fourier decomposition in proton MRI. *Magn Reson Med* 2009;62(3): 656-664.
86. Bondesson D, Schneider MJ, Gaass T, et al. Nonuniform Fourier-decomposition MRI for ventilation- and perfusion-weighted imaging of the lung. *Magn Reson Med* 2019;82(4):1312-1321.
87. Fischer A, Weick S, Ritter CO, et al. Self-gated non-Contrast-Enhanced FUncional Lung imaging (SENCEFUL) using a quasi-random fast low-angle shot (FLASH) sequence and proton MRI. *NMR Biomed* 2014;27(8):907-917.
88. Voskrebenezov A, Gutberlet M, Klimes F, et al. Feasibility of quantitative regional ventilation and perfusion mapping with phase-resolved functional lung (PREFUL) MRI in healthy volunteers and COPD, CTEPH, and CF patients. *Magn Reson Med* 2018;79(4):2306-2314.
89. Bauman G, Bieri O. Matrix pencil decomposition of time-resolved proton MRI for robust and improved assessment of pulmonary ventilation and perfusion. *Magn Reson Med* 2017;77(1):336-342.

90. Bauman G, Scholz A, Rivoire J, et al. Lung ventilation- and perfusion-weighted Fourier decomposition magnetic resonance imaging: In vivo validation with hyperpolarized  $^3\text{He}$  and dynamic contrast-enhanced MRI. *Magn Reson Med* 2013;69(1):229-237.
91. Bauman G, Lutzen U, Ullrich M, et al. Pulmonary functional imaging: Qualitative comparison of Fourier decomposition MR imaging with SPECT/CT in porcine lung. *Radiology* 2011;260(2):551-559.
92. Pohler GH, Klimes F, Voskrebenezv A, et al. Chronic thromboembolic pulmonary hypertension perioperative monitoring using phase-resolved functional lung (PREFUL)-MRI. *J Magn Reson Imaging* 2020;52(2):610-619.
93. Schonfeld C, Cebotari S, Voskrebenezv A, et al. Performance of perfusion-weighted Fourier decomposition MRI for detection of chronic pulmonary emboli. *J Magn Reson Imaging* 2015;42(1):72-79.
94. Ohno Y, Yoshikawa T, Kishida Y, Seki S, Karabulut N. Unenhanced and contrast-enhanced MR angiography and perfusion imaging for suspected pulmonary thromboembolism. *Am J Roentgenol* 2017;208(3):517-530.
95. Edelman RR, Silvers RI, Thakrar KH, et al. Nonenhanced MR angiography of the pulmonary arteries using single-shot radial quiescent-interval slice-selective (QISS): A technical feasibility study. *J Cardiovasc Magn Reson* 2017;19(1):48.
96. Ohno Y, Nishio M, Koyama H, et al. Comparison of assessment of pre-operative pulmonary vasculature in patients with non-small cell lung cancer by non-contrast-and 4D contrast-enhanced 3-T MR angiography and contrast-Enhanced 64-MDCT. *Am J Roentgenol* 2014;202(3):493-506.
97. Ohno Y, Hatabu H, Murase K, et al. Primary pulmonary hypertension: 3D dynamic perfusion MRI for quantitative analysis of regional pulmonary perfusion. *Am J Roentgenol* 2007;188(1):48-56.
98. Ley S, Mereles D, Risse F, et al. Quantitative 3D pulmonary MR-perfusion in patients with pulmonary arterial hypertension: Correlation with invasive pressure measurements. *Eur J Radiol* 2007;61(2):251-255.
99. Torres L, Kammerman J, Hahn AD, et al. Structure-function imaging of lung disease using ultrashort echo time MRI. *Acad Radiol* 2019;26(3):431-441.
100. Ma W, Sheikh K, Svenningsen S, et al. Ultra-short echo-time pulmonary MRI: Evaluation and reproducibility in COPD subjects with and without bronchiectasis. *J Magn Reson Imaging* 2015;41(5):1465-1474.
101. Roach DJ, Cremillieux Y, Serai SD, et al. Morphological and quantitative evaluation of emphysema in chronic obstructive pulmonary disease patients: A comparative study of MRI with CT. *J Magn Reson Imaging* 2016;44(6):1656-1663.
102. Pinal-Fernandez I, Pineda-Sanchez V, Pallisa-Nunez E, et al. Fast 1.5 T chest MRI for the assessment of interstitial lung disease extent secondary to systemic sclerosis. *Clin Rheumatol* 2016;35(9):2339-2345.
103. Ohno Y, Koyama H, Yoshikawa T, et al. Pulmonary high-resolution ultrashort TE MR imaging: Comparison with thin-section standard- and low-dose computed tomography for the assessment of pulmonary parenchyma diseases. *J Magn Reson Imaging* 2016;43(2):512-532.